Thermal Spray: Practical Solutions for Engineering Problems, C. C. Berndt (Ed.), Published by ASM International, Materials Park, Ohio-USA, 1996

An Investigation of Particle Trajectories and Melting in an Air Plasma Sprayed Zirconia

R.A. Neiser
Sandia National Laboratories, Albuquerque, New Mexico

T.J. Roemer
Ktech Corporation, Albuquerque, New Mexico

Abstract

The partially stabilized zirconia powders used to plasma spray thermal barrier coatings typically exhibit broad particle-size distributions. There are conflicting reports in the literature about the extent of injection-induced particle-sizing effects in air plasma-sprayed materials. If significant spatial separation of finer and coarser particles in the jet occurs, then one would expect it to play an important role in determining the microstructure and properties of deposits made from powders containing a wide range of particle sizes. This paper presents the results of a study in which a commercially available zirconia powder was fractionated into fine, medium, and coarse cuts and sprayed at the same torch conditions used for the ensemble powder. Diagnostic measurements of particle surface temperature, velocity, and number-density distributions in the plume for each size-cut and for the ensemble powder are reported. Deposits produced by traversing the torch back and forth to produce a raised bead were examined metallographically to study their shape and location with respect to the torch centerline and to look at their internal microstructure. The results show that, for the torch conditions used in this study, the fine, medium, and coarse size-cuts all followed the same mean trajectory. No measurable particle segregation effects were observed. Considerable differences in coating microstructure were observed. These differences can be explained by the different particle properties measured in the plume.

Introduction

OVER THE PAST THIRTY YEARS, thermal barrier coatings (TBC's) have grown to become one of the most important thermally sprayed materials. Their success in improving the performance of turbine engines has spurred research and development activities worldwide. A NASA workshop on TBC's in 1995 drew 200 attendees from across the United States and demonstrated the continuing high level of interest in developing better TBC's [1]. The ability of TBC's to meet challenging longer-term engine requirements necessitates an increased level of understanding of these unique materials and an unprecedented level of control over their processing.

The results presented in this paper are part of a collaborative effort between Sandia National Laboratories (Albuquerque, NM) and the National Institute of Standards and Technology (Gaithersburg, MD). The goal of this research is 1) to provide a detailed picture of the thermal and kinetic histories of a well-characterized, commercially available feedstock powder plasma sprayed under carefully controlled conditions and 2) to correlate those histories to the microstructure and properties of the resulting deposit.

In this study a commonly used agglomerated and sintered zirconia powder (Pratt&Whitney 1375 specification) was fractionated into fine, medium, and coarse portions. Each size-cut was sprayed using the same torch conditions as those used for the as-received (ensemble) powder. Particle temperature, velocity, and number-density profiles were collected both axially and radially in the plasma jet for each powder. Deposits from each powder were fabricated by sweeping the torch back and forth across a substrate to produce a raised bead. The shape of the bead, its location with respect to the torch centerline, and its microstructure were examined metallographically. The results of the metallographic examination are compared to the particle diagnostic data to develop an understanding of the role each size-fraction plays in determining the microstructure of coatings sprayed using the ensemble powder.

There is conflicting evidence in the literature regarding the extent to which particle segregation occurs during air plasma spraying. Particles injected radially into the plume penetrate to a greater or lesser extent depending on their initial momentum. Intuition would suggest that for a fixed carrier gas flow rate, coarse particles and fine particles will penetrate to different depths in the plasma jet and, therefore, follow different trajectories as they are propelled downstream. Indeed, M. Vardelle et al. have demonstrated that fine particles of aluminum oxide (15-21 μm) require a higher carrier gas flow rate than coarse aluminum oxide particles (45-90 μm) to achieve the same mean trajectory in an argon-hydrogen plasma jet [2].

DISCLAIMER

Table 1. Size distributions of zirconia powders used in this study.

Powder	*Mesh Size*	*Vol. Mean (μm)*	*Std. Dev. (μm)*	*10%< (μm)*	*25%< (μm)*	*50%< (μm)*	*75%< (μm)*	*90%< (μm)*
Fine	-400	29	11	16	22	28	36	43
Medium	-230/400	47	13	32	39	47	55	63
Coarse	-150/+230	75	20	48	65	77	88	98
Ensemble	–	53	23	25	36	52	69	84

In another study, Fincke and Swank showed that coarse particles of Ni-Al tended to cross through the plume more effectively than fine particles [3]. At an axial location 64 mm downstream of the exit plane of the torch, the average particle size they measured on the torch centerline was ~30 μm. Moving away from the centerline, the average particle size increased, becoming greater than 50 μm at a radial location of 18 mm. Interestingly, this behavior is not always observed. In a different report, Fincke and Swank showed that air plasma-sprayed zirconia did not exhibit any particle-sizing effects [4]. The radial distribution of particle size they report is flat, being ~40 μm at all locations.

Experimental Procedure

Powder Characterization. The powder used in this study was a partially stabilized zirconia (7 weight percent yttria) produced by Metallurgical Technologies, Inc. (Pearland, TX). A detailed description of the powder and a round-robin study of its particle-size distribution are presented in a companion paper [5]. The powder is a spray-dried and sintered agglomerate manufactured to meet a Pratt&Whitney 1375 specification (lot number 7YZRO-95087G-3). A portion of the powder lot was sieved into three fractions that nominally represented the finest 25 weight percent, the middle 50 weight percent, and the coarsest 25 weight percent of the as-prepared powder. These various fractions will be referred to in this paper as the "fine", "medium", "coarse", and "ensemble" powders. The fine powder was screened to a -400 mesh size (< 37 μm), the medium to a -230/+400 size-cut (37-62 μm), and the coarse to a -150/+230 (62-104 μm) size-cut.

The particle size distributions of the four powders were measured using a Coulter LS-100 particle sizer. The powder size distributions using volumetric weighting are shown in Fig. 1 and summarized in Table 1. Each powder was measured at least three times and averaged. The scatter between the separate measurements was small. When plotted on a number-density basis, all of the powders were shown to contain large numbers of tiny (micron and submicron) particles. Scanning electron microscopy (SEM) of the ensemble powder revealed that many of the agglomerated particles are *only* partially sintered (see Fig. 2.). The tiny particles are unagglomerated precursor materials used in the spray-drying process and pieces that have broken off larger, partially sintered particles.

The phase content of the four powders was examined using x-ray diffraction. As expected, the powders contained a mixture of phases (see Table 2). The relative mole fractions of monoclinic and tetragonal phases were evaluated using the x-ray technique of Miller et al. [6]. In the analysis, the concentration of cubic phase was assumed to be zero. The table also gives the ratio of the integrated intensities of the monoclinic (1 1 1) and (-1 1 1) reflections. The measured ratios compare well with a tabulated value of 0.68 [7]. The fine powder contained a substantially higher fraction of monoclinic phase than did either the medium or coarse powders. The reason for this higher concentration is not known. The mole fraction of the monoclinic phase in the ensemble powder reported by the

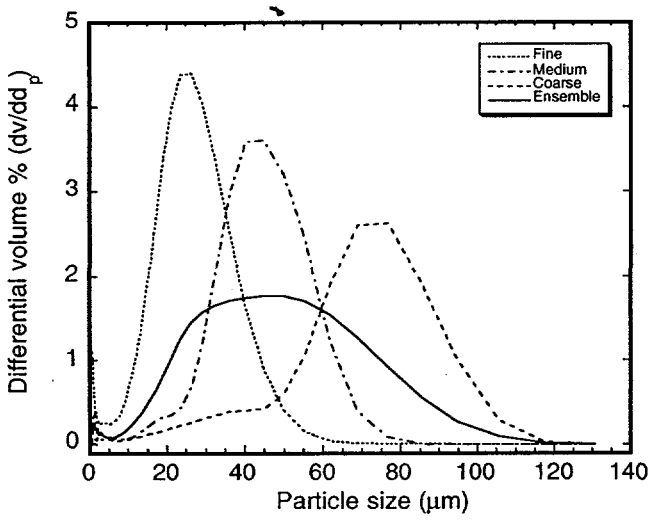

Fig. 1 - Size distributions of fine, medium, coarse and ensemble zirconia powders.

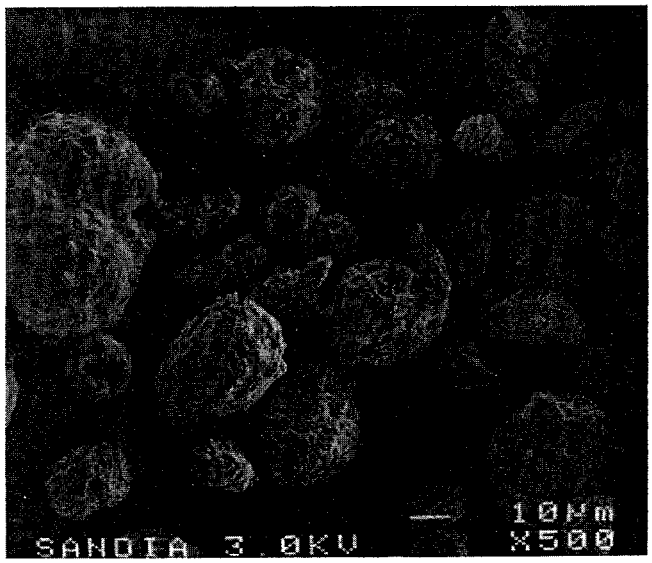

Fig. 2 - SEM micrograph of ensemble powder.

Table 2. X-ray diffraction data from zirconia powders and coatings.

	Monoclinic Mole %	*Intensity Ratio (111) / (-111)*
Fine Powder	52	0.65
Medium Powder	43	0.68
Coarse Powder	40	0.66
Fine Coating	12	0.49
Medium Coating	3	0.55
Coarse Coating	13	0.62
Ensemb. Coating	7	0.58

manufacturer in its certification package was ~42%, in reasonable agreement with expectations based on Table 2.

Processing Conditions. A Miller Thermal SG-100 plasma spray torch was used to spray the zirconia. The torch hardware consisted of a 730 anode, a 720 cathode, and a 112 gas injector ring. The 112 gas injector is a straight injector (i.e., no swirl component is given to the plasma-forming gas). Powder was internally injected through a 1.8 mm diameter port located 12 mm from the front face of the torch. The port forward-injects the powder at an angle ~18° off-normal. Table 3 lists the torch operating conditions used in this study. The spraying was performed at 83.3 kPa (Albuquerque, NM). The total power into the torch was 33 kW. At these settings,

Table 3. Torch operating conditions.

Arc gas - Ar	39 SLPM
Aux gas - He	22 SLPM
Carrier - Ar	1.9 SLPM
Arc current	950 A
Arc voltage	35-36 V
Efficiency	50-55%
Feed Rates	
Fine	4.6 g/m
Medium	9.8 g/m
Coarse	10.5 g/m
Ensemble	8.6 g/m

the torch was 50-55% efficient (i.e., 45-50% of the total power was lost to the coolant). The largest uncertainty in the net power calculation was the accuracy of the water flow rate measurement, which may be as much as 10% in error.

The gas flow rates were measured using pressure transducers and jeweled critical orifices calibrated using a primary standard at Sandia. The helium and argon were technical grade (99.99% and 99.995% purity, respectively). A new electrode set was used during the particle temperature and velocity measurements. The electrodes were first "broken in" by running them for 30 minutes using an argon-only plasma at 40 SLPM and 500 A. During the course of the diagnostic measurements, the gun voltage was 36.0±0.1 V. This electrode set became damaged after the diagnostic measurements were

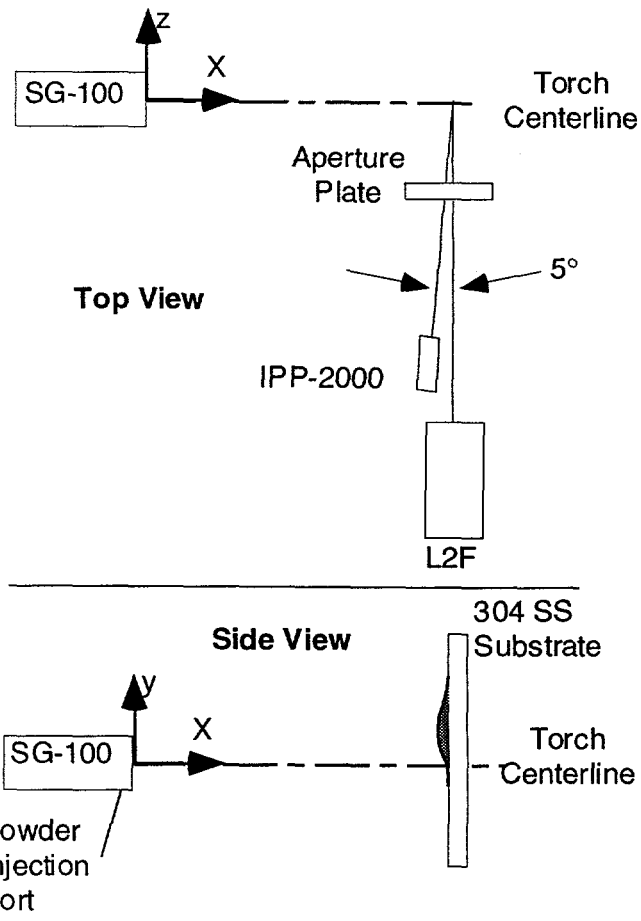

Fig. 3 - Schematic diagram of experimental setup. Substrate was not present during particle diagnostic measurements.

completed but before the coatings examined in this report were sprayed. As a result, a second electrode set was broken in and used to spray the coatings. Despite being nominally the same as the first set, this second set operated at a slightly lower voltage (35.0 V). However, the temperature difference between the water cooling lines was slightly less, too, resulting in similar net powers for both sets of electrodes.

Particle Diagnostics. Measurements of particle velocity and temperature were made both axially and radially in the jet for each of the four different powders. The SG-100 was mounted onto a computer-controlled milling machine. Particle velocity distributions were measured using a laser two-focus (L2F) velocimeter [8]. Particle count rates from the velocimeter provide a measure of the spatial distribution of particles in the jet. Particle temperatures were determined using an IPP 2000 two-color pyrometer manufactured by Inflight (Idaho Falls, ID). A description of the device and its performance is available in the literature [9]. A schematic diagram of top and side views of the setup are shown in Fig. 3. An xyz coordinate system is shown with the origin located at the center of the hole in the exit plane of the torch. The side view shows that particles were injected from the bottom of the torch in the x-y plane along a direction close to the y-axis but inclined slightly in the +x direction (i.e., with forward injection).

The L2F and IPP-2000 were aligned to point at the same

location in the jet. The L2F was aligned parallel to the z-axis. The IPP-2000's optical axis was in the x-z plane and tilted at a 5° angle with respect to the L2F axis as shown in Fig. 3. An optically black stainless steel aperture plate located ~40 mm from the torch centerline was used to limit the field of view of the IPP-2000 to ~1 mm. Diagnostic measurements were made axially in 10 mm steps from 40 to 140 mm downstream of the exit plane of the torch. The measurements were made along a line displaced upwards by 2 mm (i.e., y=+2 mm). The measurements were displaced upwards in order to stay within the densest portion of the particle stream. Radial measurements were made in 2 mm steps over the range y=±10 mm at an axial location of x=100 mm. During the particle diagnostic measurements, there was no substrate present. After the diagnostic measurements were completed, the diagnostics were removed and a substrate fixture was set up at x=100 mm.

The IPP-2000 was calibrated in-situ using a tungsten strip-lamp standard. A gray-body assumption (i.e., constant emissivity) was made in converting the voltage ratio from the two detectors to a temperature. At each measurement location in the jet, two sets of measurements were made. The first with the powder off to determine the background signal strength, and the second with the powder on. The background measurements were subtracted before a temperature was calculated. Except for the measurement made at x=40 mm where the plume was still very bright, the background signal strengths were well below 10% of the powder-on signal. At each location, 100 measurements were made at a rate of ~10 Hz. The standard deviation in these 100 measurements was less than 1%. The fine powder tended to pulse somewhat during spraying, and the voltages in the two IPP-2000 channels fluctuated considerably; however, the voltage ratio remained quite stable.

Particle velocity measurements made near the torch centerline typically lasted about 10 seconds, resulting in distributions containing 5000-10000 separate measurements. Near the edges of the radial scans, measurements took ~30 seconds. Velocity distributions containing fewer than 600 measurements were rejected.

Coating Preparation. Grit-blasted 304 stainless steel strips (12.7 mm wide x 100 mm long x 1.6 mm thick) were placed 100 mm downstream of the exit plane of the torch with their long dimension parallel to the y-axis (see Fig. 3 side view). Three coupons were prepared simultaneously for each of the four powders. A scribe line across the back of each coupon was aligned with the torch centerline. Coatings were deposited by translating the torch back and forth along the z-axis to produce a raised bead. The torch was traversed a total of 80 times across the coupons at a rate of 220 mm/s. Weight-gain measurements were used to determine deposition efficiencies (see Table 4). The impact angle for droplets striking the steepest slope on the side of the bead was ≤5° off-normal with respect to the substrate surface, so effects of deposition angle on porosity, deposition efficiency, and surface roughness should be minimal [10].

The coatings deposited using the fine powder were tan/gray in color, while the coarse material retained the yellow color of the feedstock powder. The color change results from a slight reduction of the zirconia during spraying. A short exposure to elevated temperatures in air returns the coating to its yellow color [11].

In addition to the steel strips, 50 mm x 50 mm coupons were coated in a second set of spray runs for x-ray analysis. In this set of runs, the torch was rastered in the y-z plane to produce flat coatings.

Coating Characterization. The coated stainless steel strips were sectioned metallographically to examine the shape of the bead and the porosity within it. One of the three strips sprayed for each powder was vacuum impregnated in Shell Epon 828 epoxy (diethanolamine hardener) and cured in air overnight at 85°C. The potted strips were then sectioned with a slow-speed diamond saw at two locations. The first cut was made ~6 mm below the torch centerline scribe mark (i.e., at y=-6 mm), and the second was made at y=+20 mm. After remounting the sectioned strips, they were ground using a series of diamond-lapping platens. The ground cross-sections of the beads were vibratory polished using a nylon cloth and colloidal silica. Grinding and polishing operations were performed simultaneously on all the specimens to ensure uniformity in their processing.

Coating thickness as a function of distance from the torch centerline was measured at 250 μm intervals. Porosity measurements were made using the image analysis package Prismview (v 2.2) from Dapple Systems, Inc. (Sunnyvale, CA). The measurements were made at 200x in green light using the same gray-scale limits for each specimen. A total of 10 measurements were made in each sample at various locations within the bead. The standard deviation of the 10 measurements was ~10% of the mean for all four specimens.

A second set of the beads was gold-coated and examined in the SEM. The morphology of the deposited coating was examined at 4 mm increments from y=-8 mm to y=+8 mm.

X-ray diffraction measurements were made on the 50 mm square coupons to determine the relative amounts of tetragonal and monoclinic phases in the as-sprayed deposits. The results of this analysis are given in Table 2.

Results

Characteristics of the Particle Plume. Particle-velocity distributions for the four powders measured at x=100

Table 4. Characteristics of sprayed deposits (beads).

Coating	*Wt. Gain (g)*	*DE (%)*	*Max. Thickness (μm)*	*Area (sq. cm)*	*Centroid (mm)*	*FWHM (mm)*	*Porosity (%)*
Fine	0.18	51	310	0.024	3.3	7.3	4
Medium	0.38	51	860	0.056	2.8	6.0	9
Coarse	0.28	35	820	0.046	3.4	5.3	20
Ensemble	0.34	52	750	0.051	3.5	6.3	14

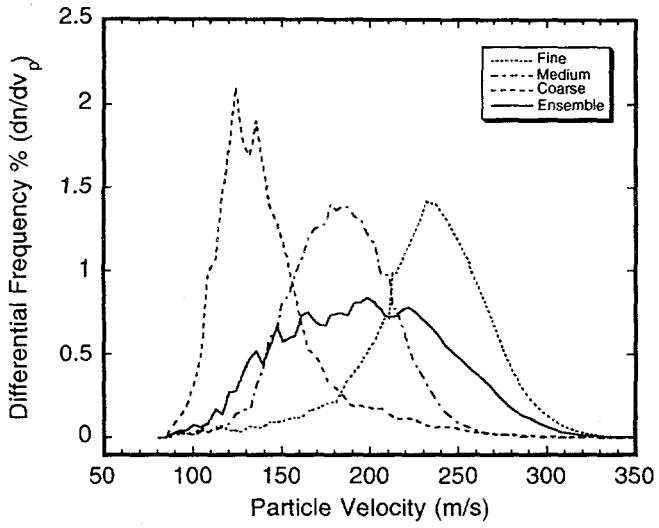

Fig. 4 - Particle velocity distributions recorded at x=100 mm, y=+2 mm.

mm, y=+2 mm are shown in Fig. 4. The mean velocities of the fine, medium, and coarse powders at this location were 239, 186, and 143 m/s respectively. The velocity distribution for the ensemble particles is much broader, as expected, and has a mean value of 201 m/s. In agreement with simple theory, the mean particle sizes of the three size-cuts (see Table 1) are inversely proportional to the square of mean particle velocity [12]. This behavior has been widely observed in powder-fed thermal-spray torches.

Mean particle velocity as a function of axial position is shown in Fig. 5. Velocities for the medium and coarse powders remain relatively unchanged over the entire measurement range. The fine powder reacts more rapidly to the decay of the gas jet, and its mean velocity decreases steadily from 250 m/s to 210 m/s. The more complex behavior of the ensemble powder probably results from its wide-size distribution and the different rates at which various particle sizes penetrate the jet.

Figure 6 shows that the surface temperatures of the particles drop off continuously as they travel down the plume. The surface temperature drops as heat is lost to the surroundings and is conducted into the particle. The average surface temperature of the fine particles is above the melting temperature at all locations while the coarse particles hover around the melting temperature of ~3000K.

Care must be taken not to interpret these temperatures too rigidly. Fincke and Swank have shown that substantial numbers of unmelted particles are present when zirconia is air plasma sprayed [4]. Large numbers of these particles can be present without affecting the temperature observed with the IPP-2000.

Interpretation of the particle temperature data is further complicated by the poor thermal conductivity of zirconia. Theoretical calculations by Bourdin et al. show that a steep temperature gradient will exist between the surface and the core of a zirconia particle because heat is deposited on the surface of the particle much faster than it can be conducted into the interior [13]. The time required for the center of the particle to approach the surface temperature typically exceeds the dwell time of the particles in the jet. Calculations presented by M. Vardelle et al. demonstrate that this is particularly true for agglomerated zirconia particles since they have a lower conductivity as compared to the fully dense particles assumed by Bourdin et al. [14].

Since very little superheating of the surface of the coarse particles is observed in Fig. 6 and strong temperature gradients are sure to exist within the particles, it is clear that the coarse particles can not be fully molten. The low deposition efficiency, high porosity levels and rough surface of the coarse coating support this conclusion. Conversely, the very high surface temperatures recorded for the fine particles and their shorter homogenization times indicate that significant melting of the fine particles does occur.

Particle temperature, velocity, and count rate data taken radially at x=100 mm are shown in Figs. 7-9. The particle count rates show that the fine, medium, and coarse powders do not become spatially segregated to any significant extent for the conditions used in this study. The peak count rate occurred at y=+4 mm for all four powders. The count rate dropped off rapidly at the top of the plume, but exhibited a slowly falling tail that extended well below the torch centerline on the bottom.

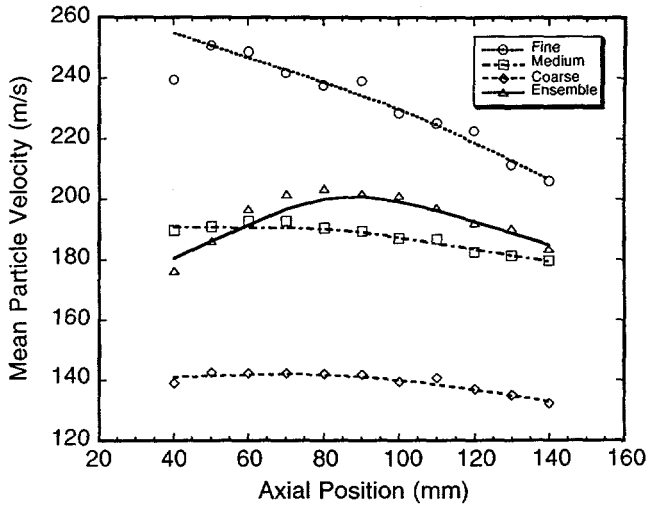

Fig. 5 - Mean particle velocity vs. axial position.

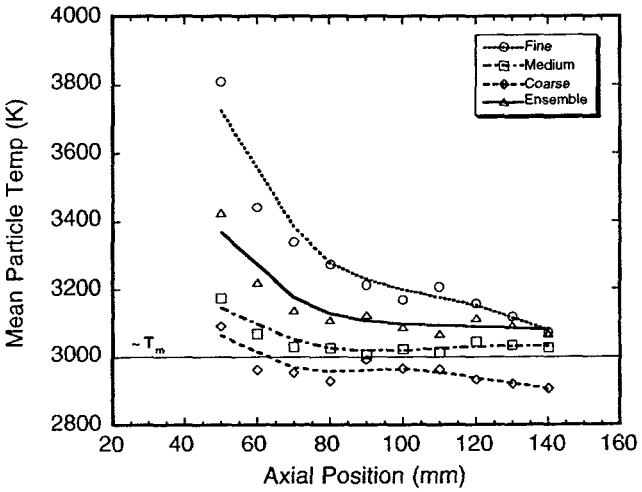

Fig. 6 - Mean particle temperature vs. axial position.

Deposit Shapes. The cross-sectional shapes of the deposits sprayed onto the stainless steel strips are shown in Fig. 10 a-d. The maximum thickness of the coatings has been normalized to unity so it can be compared more easily to the normalized particle count rate data from the L2F superimposed on the plots. Values for the centroids, maximum thicknesses, cross-sectional areas, and full-width-half-maximums (FWHM) of the distributions are given in Table 4. The deposits are very symmetrical about their mean positions and, interestingly, are quite close to Gaussian in shape. Within experimental error, the centroid positions of the four deposits are the same. The FWHM of the bead sprayed using the fine powder was 2 mm (~40%) wider than the bead deposited using the coarse powder. The medium and ensemble powders had intermediate widths.

Deposit Microstructures. Metallographic examination showed that the fine deposit was denser than the medium deposit which, in turn, was considerably denser than the coarse deposit. The porosities determined by image analysis are listed in Table 4. These values agree well with approximate bulk densities determined by dividing the weight gain of the coupon by the volume of the sprayed deposits (cross-sectional area x bead length) and by the density of zirconia (5.86 g/cc). SEM images (Fig. 11) of the top surfaces of the deposits confirmed that the fine powder was much better melted than the coarse powder, in agreement with expectations based on the particle temperature measurements in Figs. 6 and 7. Unmelted pieces of the agglomerated feedstock particles are the dominant feature on the surface of the coarse specimen (Fig. 11c). Unmelted particles are present in the fine specimen as well; however, they are for the most part embedded in well-melted material (Fig. 11a).

Two dominant types of porosity were observed in the optical microscope. Both are associated with unmelted particles. One type appears underneath and beside partially melted particles. It occurs because there is insufficient liquid available to completely fill the voids at the point of impact, leaving behind empty cavities that can be tens of microns across. Similar porosity has been observed in coatings made from incompletely melted tungsten [15]. The second kind of porosity appears within the unmelted core of coarse particles (see Fig. 12). The porosity is present because of the skeletal, incompletely sintered nature of the feedstock material. This porosity is, of course, smaller in size and was most common in the coarse coating.

The four deposits were examined for any noticeable changes in microstructure from the bottom to the top of the bead. Over the continuously coated portions of the fine, medium, and coarse deposits, no discernible differences in the amount or morphology of the porosity were observed. The ensemble specimen seemed to be somewhat denser at the edges of the deposit than in the center. However, the coating was not thick enough in these regions to reliably quantify the difference using image analysis. More measurements are needed to confirm this observation. The fine powder interacts more strongly with turbulent eddies in the jet than the coarse powder and spreads out to produce a wider particle plume, and hence, a wider bead. On this basis, one would expect that the edges of the ensemble powder's particle plume would contain a higher fraction of fine material, resulting in a denser deposit.

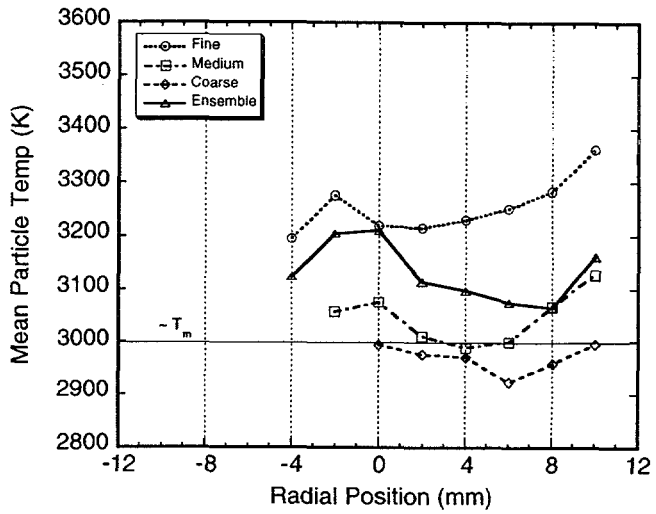

Fig. 7 - Mean particle temperature vs. radial position.

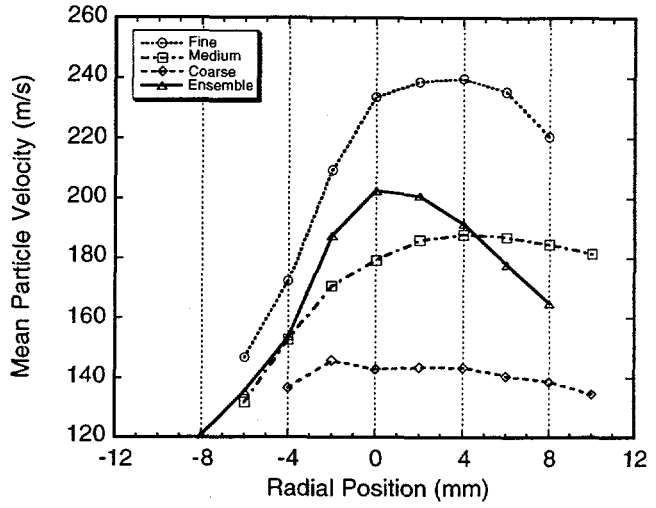

Fig. 8 - Mean particle velocity vs. radial position.

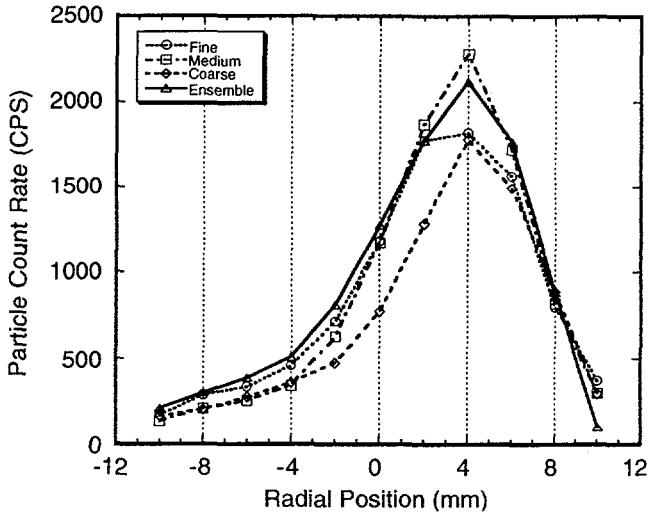

Fig. 9 - Particle count rate vs. radial position.

This segregation phenomenon affects a relatively small fraction of the total volume of the deposit, and it seems unlikely that it would have a significant effect on the performance of coatings sprayed with the ensemble powder.

Deposit Phase Content. Molten zirconia that is rapidly quenched will crystallize as tetragonal zirconia and will not transform to the monoclinic phase as it cools down, provided it contains sufficient stabilizer. X-ray diffraction patterns collected from the 50 mm square plates showed that the mole fraction of monoclinic phase in the sprayed deposits was much less than in the feedstock powders (see Table 2). The coating sprayed with the fine powder contains more monoclinic phase than the coating sprayed with the medium powder. However, this observation is not unreasonable since the fine powder contained more monoclinic material than the medium powder to begin with.

The ratio of the monoclinic (1 1 1) and (-1 1 1) diffraction lines is less than the 0.68 value observed in the powders. The ratio is smallest for the fine coating and greatest for the coarse (see Table 2). The cause of this reduction is uncertain, but it may indicate that some textured monoclinic material is formed during spraying. One can reasonably expect that unmelted particles such as those in Fig. 11 will be randomly oriented with respect to the substrate surface. Therefore, if unmelted particles were the sole source of the monoclinic signal, the same 0.68 ratio observed in the feedstock powder should be seen in the coatings. Since the powder is a spray-dried and sintered agglomerate of zirconia and yttria, the yttria stabilizer will not be uniformly dispersed within each particle that makes up the agglomerate. Pockets of yttria-rich and yttria-poor material will exist. Not all of the molten and partially molten particles of yttria-deficient zirconia will contain enough stabilizer to prevent the tetragonal to monoclinic transformation from occurring as the splat cools. Monoclinic phase transformed from the rapidly solidified tetragonal phase could quite possibly be textured and would explain the lower-than-expected integrated intensity ratio observed in the sprayed coatings.

Discussion

All four of the raised beads deposited using the various powder cuts were centered on a position about 3 mm above the torch centerline. This position is within a millimeter of the peak in the particle flux measured using the laser velocimeter. The majority of the deposited material spans the range from y=0 to y=+7 mm. Figures 7 and 8 show that the particle temperatures and velocities are uniform over that range. This is an important observation because, taken in combination with the fact that the fine, medium, and coarse powders did not separate spatially in the plume, it indicates that the microstructure of the deposit produced at these spray conditions should be uniform across the width of the bead. This hypothesis is in agreement with our observations of coating microstructure.

Fincke and Swank have made particle diagnostic measurements on air plasma-sprayed zirconia [4]. In their study, they fed a spray-dried and sintered zirconia having a similar size distribution to the ensemble powder into a Miller SG-100 torch. The plasma gas flow rates, torch power level, and nozzle geometry were close to the ones used here. However, their

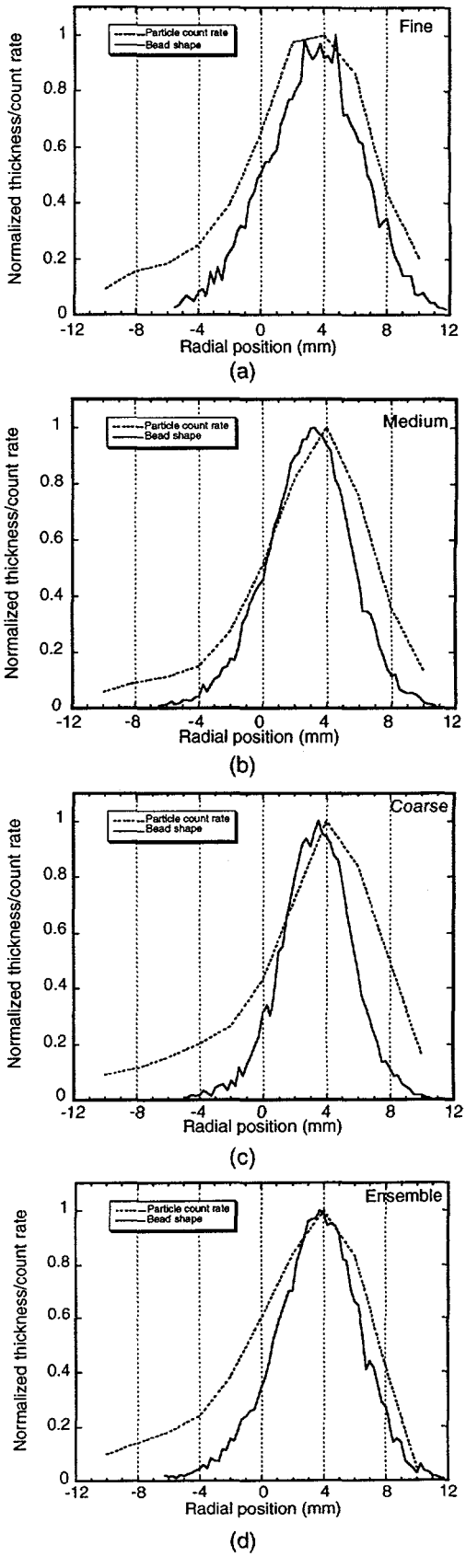

Fig. 10(a-d) - Shape of deposited bead and particle count rate vs. radial position for the four different powders.

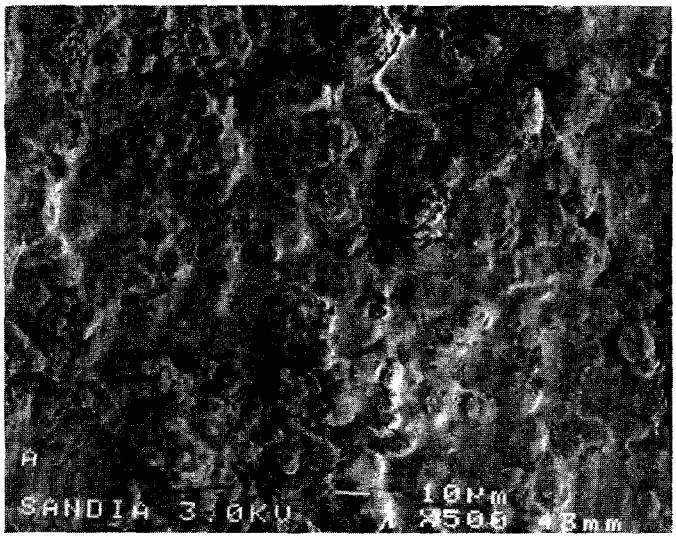

(a) Fine

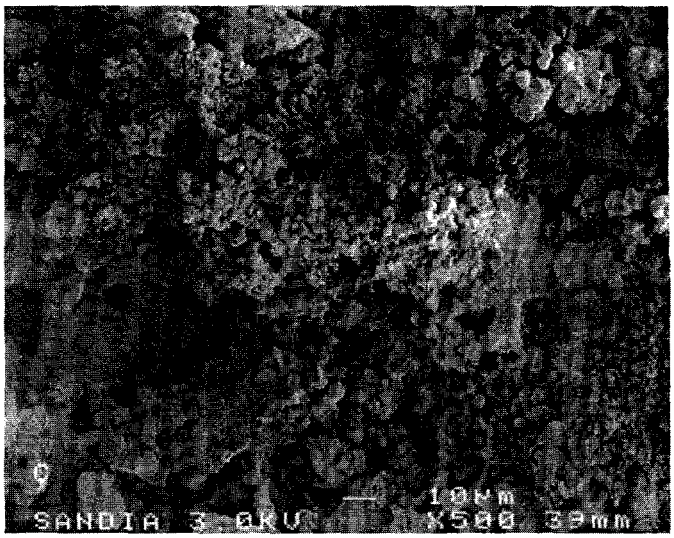

(c) Coarse

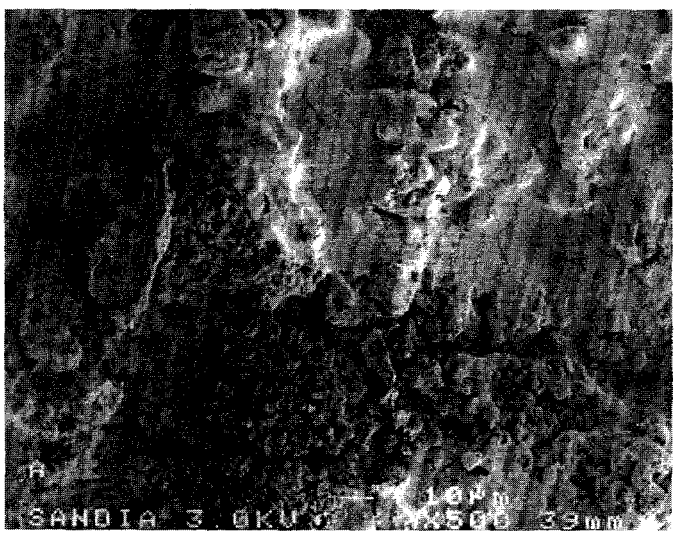

(b) Medium

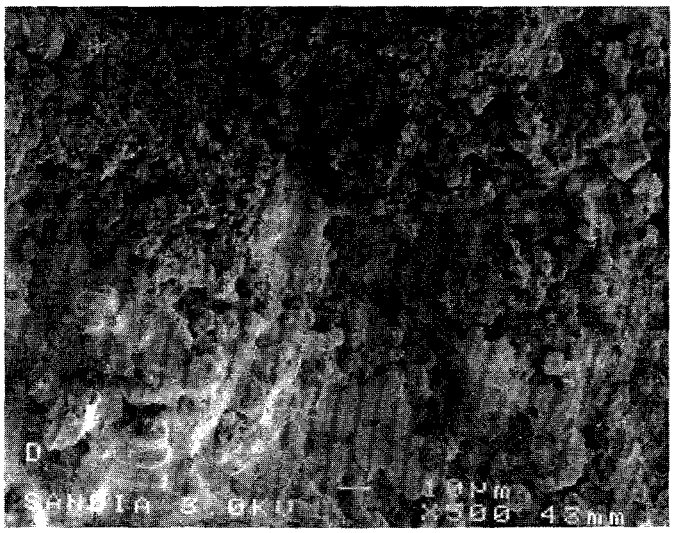

(d) Ensemble

Fig. 11(a-d) - SEM micrographs of the top surfaces of the sprayed beads taken at a radial location of y=+4 mm.

carrier gas flow rate was 6.1 SLPM and they used back-injection as compared to the 1.9 SLPM and forward-injection used here. Because of the these changes to the particle injection process, the particles in their study were pushed almost a centimeter further through the plume. They measured the average particle size as a function of radial position at x=120 mm and found that it was essentially constant over the range y=0 mm to y=+24 mm. That is to say, despite the substantially greater penetration achieved by the particles in their study, they did not observe any apparent injection-induced particle-sizing effects either.

An examination of Fig. 10 shows that the shape of the bead deposited by the torch matches the particle flux distribution to a considerable extent. However, at the bottom of the plume, beginning near the torch centerline and extending downward, the thickness of the deposited material drops off significantly faster than the particle count rate does. The particles comprising the tail of the particle flux distribution are believed to be the very fine micron-sized particles present in large numbers in all four powders. M. Vardelle et al. have shown these fine bits of unagglomerated zirconia fail to penetrate into the core of the jet; instead, they become a slow moving cloud of tiny particles that travel in the periphery of the jet [14]. In agreement with this observation, Fig. 8 shows that particle velocities below the centerline of the plasma jet are dropping rapidly. Moreover, SEM images taken at y=-8 mm revealed the presence of a dusting of unmelted micron- and submicron-sized particles on the substrate surface.

Conclusions

The trajectories, temperatures, and velocities of the small, medium, and large particles comprising a typical commercially available zirconia powder during air plasma spraying are reported. Particle temperature measurements along the jet

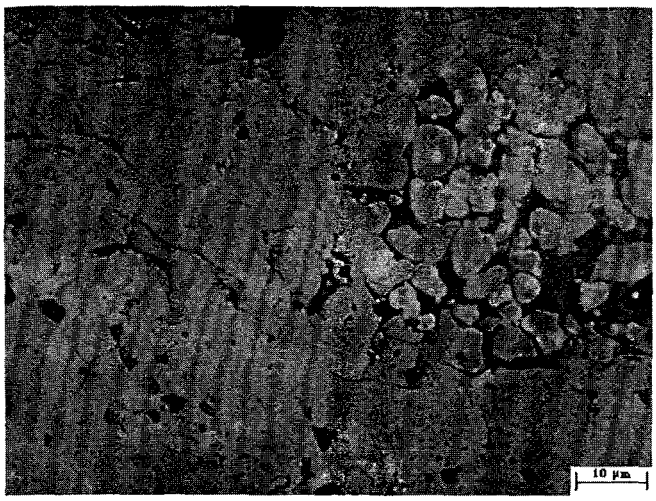

Fig. 12 - Optical micrograph of ensemble deposit showing an unmelted particle and the porosity within it.

axis revealed that the coarse powders were largely unmelted by the plasma jet. Fine particles melted much more completely. Not surprisingly, the deposition efficiency of the fine material was substantially greater than the coarse material, and the porosity of coatings produced with the fine material was substantially less. The porosity observed in coatings sprayed from the ensemble powder is largely due to unmelted coarse particles. The fine particles are better melted and give the deposit mechanical strength.

Within the accuracy of the alignment of our equipment, there were no differences in the mean trajectories taken by the fine, medium, and coarse powders in the plume in reaching an axial location of 100 mm. Over the range of radial locations where material is deposited, the surface temperatures and velocities of the fine, medium, and coarse particles were very uniform. As a result, no discernible differences in coating microstructure were observed over the width of the beads laid down by the three powder fractions. The fine particles are spread over a wider range of trajectories than the coarse particles, and the bead produced by the fine particles is broader. However, this seems to have at most a minor effect on the microstructure of the ensemble coatings. Extremely fine (micron-sized) bits of unagglomerated material and broken pieces of incompletely sintered agglomerates fail to penetrate into the plume and become a slow-moving cloud of cold particulate at the bottom of the jet. The volume fraction of this material is extremely small and is not believed to have any effect on the microstructure or properties of the sprayed coatings.

Acknowledgments

The authors would like to thank several individuals for their important contributions to this effort. At Sandia, Ray Cote operated the torch and produced the coatings; Robert Johnston helped set up the experiments and take the data; Andy Mayer modified the data acquisition and analysis software; Dale McGuffin performed the metallography; Mark Rodriguez collected the diffraction data; and Gary Zender operated the SEM. Their assistance is greatly appreciated. The authors also wish to thank Mark Smith at Sandia, Jim Huddleston at Metallurgical Technologies, Robert Miller at NASA LERC, and Patrick Pei and Sandy Dapkunas at NIST for helpful discussions.

Sandia National Laboratories is operated by Lockheed Martin for the U.S. Department of Energy under contract DE-AC04-94AL85000.

References

1. Thermal Barrier Coating Workshop Conference Proceedings, W.J. Brindley, ed., NASA Conference Publication 3312, Cleveland, OH, March 27-29, 1995.
2. M. Vardelle, A. Vardelle, and P. Fauchais, J. Thermal Spray Tech., 2, 79, (1993).
3. J.R. Fincke and W.D. Swank, Proc. 4th National Thermal Spray Conf., T.F. Bernecki, ed., Pittsburgh, PA, May 4-10, 1991, p.193.
4. J.R. Fincke and W.D. Swank, Proc. International Thermal Spray Conf., C.C. Berndt, ed., Orlando, FL, May 28-June 5, 1992, p.513.
5. P. Pei, J. Kelly, S. Malghan, and S. Dapkunas, "Analysis of Zirconia Powder for Plasma Spray", Proc. 9th National Thermal Spray Conf., Cincinnati, OH, Oct. 7-11, 1996.
6. R.A. Miller, J.L. Smialek, and R.G. Garlick, Adv. in Ceramics, 3, 241, (1981).
7. Card 37-1484, PDF database, International Centre for Diffraction Data, Newtown Square, PA.
8. M.F. Smith, T.J. O'Hern, J.E. Brockmann, R.A. Neiser, and T.J. Roemer, Proc. 8th National Thermal Spray Conf., C.C. Berndt and S. Sampath, eds., Houston, TX, Sept. 11-15, 1995, p.105.
9. W.D. Swank, J.R. Fincke, and D.C. Haggard, Proc. 8th National Thermal Spray Conf., C.C. Berndt and S. Sampath, eds., Houston, TX, Sept. 11-15, 1995, p.111.
10. M.F. Smith, R.A. Neiser, R.C. Dykhuizen, Proc. 7th National Thermal Spray Conf., C.C. Berndt and S. Sampath, eds., Boston, MA, June 20-24, 1994, p.603.
11. S. Sampath, SUNY Stony Brook, Stony Brook, NY, private communication.
12. R.A. Neiser, J.E. Brockmann, T.J. O'Hern, R.C. Dykhuizen, M.F. Smith, T.J. Roemer, R.E. Teets, Proc. 8th National Thermal Spray Conf., C.C. Berndt and S. Sampath, eds., Sept. 11-15, 1995 Houston, TX, p.99.
13. E. Bourdin, P. Fauchais, and M. Boulos, Int. J. Heat Mass Transfer, 26, 567, (1983).
14. M. Vardelle, A. Vardelle, A. Denoirjean, and P. Fauchais, Proc. 1989 International Thermal Spray Conf., I.A. Bucklow, ed., June 4-9, 1989, London, UK, p. P49-1.
15. R.A. Neiser, R.D. Watson, G.R. Smolik, and K.J. Hollis, Proc. 5th National Thermal Spray Conf., C.C. Berndt and T.F. Bernecki, eds., June 7-11, 1993, Anaheim, CA, p.303.